Article

Synergic Role of Self-Interstitials and Vacancies in Indium Melting

Roberto Montanari * and Alessandra Varone

Department of Industrial Engineering, University of Rome-Tor Vergata, Via del Politecnico 1 00133, Rome, Italy; E-Mail: alessandra.varone@uniroma2.it

* Author to whom correspondence should be addressed; E-Mail: roberto.montanari@uniroma2.it; Tel.:+39-0672597182; Fax: +39-06-20-21-351

Abstract: Precursor effects of indium melting have been investigated by means of Mechanical Spectroscopy (MS) and High Temperature X-ray Diffraction (HT-XRD). MS tests evidenced a sharp drop of dynamic modulus in the temperature range between 418 K and 429 K (melting point). At 429 K, HT-XRD showed partial grain re-orientation, peak profile broadening, in particular in the lower part, and peak shift towards lower angles. Experimental results are consistent with density increase of self-interstitials and vacancies in the crystal lattice before melting. Self-interstitials and vacancies play a synergic role in the solid–liquid (S-L) transformation. The increase of self-interstitials over a temperature range of about 10 K before melting has the effect of weakening interatomic bonds (modulus drop) that favors the successive vacancy formation. Finally, the huge increase of vacancy concentration above 428 K leads to the collapse of crystal lattice (melting).

Keywords: indium; precursor phenomena of melting; dynamic modulus; high temperature X-Ray diffraction; self-interstitials; vacancy

1. Introduction

Melting of pure metals has been extensively investigated in the past [1]. Since the discovery of the empirical Lindemann's criterion [2] stating that melting occurs if the average atomic vibration

amplitude exceeds a certain value (about 10% of the distance between nearest neighbors), many investigators have tried to find out the microscopic precursor mechanisms leading to crystal melting.

In 1939, Born proposed a theory based on the assumption that a liquid has zero resistance to shear stress [3]. Atomic distances increase with temperature; thus, the restoring forces between the atoms are reduced as well as the shear elastic moduli leading to a structural instability of the solid and finally to its collapse at a critical temperature. However, successive measurements of Hunter and Siegal [4] showed that the values of shear elastic moduli decrease but are nonzero at the melting point, so the Born's approach was modified by Tallon [5] to get a better agreement between theoretical and experimental results. For some decades, the favorite picture was the softening of a phonon mode due to thermal fluctuations, but this model has a clear shortcoming: in real crystals, several defects such as dislocations, self-interstitial atoms and vacancies, are excited well below the melting point T_M.

The role of defects in the melting mechanism was first understood by Gorecki [6], who stressed the correlation between bonding energy of metals and vacancy formation energy.

A model of historical relevance is due to Kuhlman–Wilsdorf [7]: the theory is based on the contention that melting occurs when the free energy of dislocation cores assumes negative values. Some years later, Weber and Stillinger [8] focused the attention on point defects and developed a statistical model of melting based on the cooperative formation of vacancy–interstitial pairs.

Granato [9] derived an interstitial-concentration-dependent free energy, appropriate for calculation of all the thermodynamic properties of crystalline and liquid states of metals. The theory predicts that the shear elastic modulus decreases when the concentration of self-interstitials increases.

More recently, melting has been investigated by Monte Carlo computer simulations [10–12]. Gomez *et al.* [11,12] evaluated the percentage of defects near T_M and showed that defects form clusters, which are not isolated, but rather linked over long distances near the phase transition. In fact, their calculations indicate that the linked clusters are dislocations and melting is consistent with the saturation of the crystal by dislocation loops. Molecular-dynamics investigations of Lutsko *et al.* [13] and Sinno *et al.* [14] showed that extrinsic defects are the dominant mechanism for the initiation of melting. In particular, the Stillinger–Weber interatomic potential has been used to estimate the equilibrium and transport properties of self-interstitials and vacancies in Si [14] and equilibrium configurations were predicted as a <110> dumbbell for a self-interstitial, and as an inwardly relaxed configuration for vacancies. It was found that both structures show considerable delocalization with increasing temperature, which leads to a strong temperature dependence of the entropy of formation.

This work investigated the melting of pure In and its precursor phenomena by Mechanical Spectroscopy (MS), *i.e.*, internal friction (IF) and dynamic modulus measurements, and high temperature X-ray diffraction (HT-XRD). The MS technique and its applications to solid-state physics and materials science are discussed in some classical texts [15,16]. It is noteworthy to remind that few data from MS tests on liquid metals are reported in the literature [17] and have been obtained by means of a modified inverted torsion pendulum operated by forced oscillations. The present experiments have been done by using a new method developed by us [18,19]; it operates in resonance conditions and employs hollow reeds of stainless steel containing the liquid metal.

HT-XRD permitted to correlate MS data with the structural features of solid and liquid phases as temperature increases up to T_M and above.

2. Materials and Experimental

The investigated material was In with purity of 99.999 wt %. All the samples for HT-XRD measurements have been prepared by slowly cooling from the melt for minimizing the defective structures. Two sets of samples (A and B) with different grain orientation have been examined: set A had a strong {002} texture, set B a strong {101} texture.

HT-XRD measurements have been carried out by means of an ANTON PAAR HT-16 camera (Graz, Austria) with a sample holder apt to contain molten metals in an atmosphere of inert gas. Diffraction patterns have been collected with Mo-Kα radiation (λ = 0.7093 Å) at increasing temperatures with steps of 5 K from room temperature up to 420 K and with steps of 1 K from 420 K to the melting point (T_M = 429 K). During each test, the temperature, controlled by a thermocouple embedded into the sample, was maintained constant (±0.1 K). In order to determine the lattice spacings d_{hkl} and the volume of unit cell *V* with good precision, the tests were carried out with 2Θ angular intervals of 0.005 ° and counting times of 10 s per step. The unit cell of In is tetragonal body centered; thus, its volume $V = a^2 c$, with *a* and *c* the axis lengths; *a* and *c* are calculated by introducing in Equation (1) a couple (at least) of different d_{hkl} values.

$$d_{hkl} = \left[\frac{h^2 + k^2}{a^2} + \frac{l^2}{c^2} \right]^{-1/2} \tag{1}$$

XRD spectra of melt have been recorded by step-scanning in the 2Θ angular range 5 °–55 ° with steps of 0.05 ° and counting time of 5 s per step. From the diffraction pattern of melt, the radial distribution function (RDF) curve, $4\pi r^2 \rho(r)$, was calculated. It represents the average number of atom centers between the distances *r* and *r* + d*r* from the center of a given atom; for a mono-atomic liquid, the RDF can be expressed as:

$$4\pi r^2 \rho(r) = 4\pi r^2 \rho_0 + \frac{2r}{\pi} \int_0^\infty Q i(Q) \sin(Qr) \mathrm{d}Q \tag{2}$$

where $Q = 4\pi \sin\Theta / \lambda$ and ρ_0 is the mean density, *i.e.*, the average number of atoms per unit volume. The calculation of the function $i(Q)$ in Equation (2), and more in general, the analytic method to determine the RDF have been described in detail elsewhere [20].

MS experiments have been made by using reeds mounted in free-clamped mode and excited by flexural vibrations. In was cast inside a hollow reed of stainless steel (AISI 316) closed to an end. Great attention was paid to get a complete filling of the reed because the presence of air bubbles may introduce spurious energy loss and affect the experiments. Finally, after the In solidification, the open extremity of the reed was sealed. AISI 316 steel melts at a much higher temperature than those involved in present experiments, so the method permits studying liquid metals in the same way commonly used for solid ones. Of course, experimental data have been corrected from the contribution of the container measured by tests in the same conditions using not filled reeds (Figure 1). The elastic modulus *E* is normalized to the initial value E_0. The Q^{-1} curve represents the energy loss contribution from the container, which is subtracted from experimental data to get the effective curves.
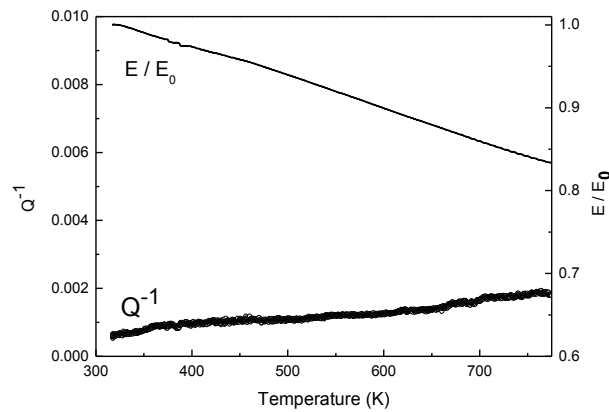
Figure 1. Trends of Q^{-1} and E/E_0 determined in tests carried out on hollow reeds of AISI 316 steel.

MS experiments were carried out by means of the mechanical analyzer VRA 1604 (CANTIL Srl, Bologna, Italy) [21]. Q^{-1} values have been determined from logarithmic decay of flexural vibrations. The resonance frequency f was in the range of KHz; the strain amplitude was kept lower than 1×10^{-5}. The samples have been heated from room temperature to 466 K, *i.e.*, above T_M, with constant rate of 8.3×10^{-3} K s^{-1}. Another group of tests have been made around T_M, in the temperature range 410–440 K, in conditions of thermal equilibrium after soaking the samples for 1.8×10^3 s at the test temperature. The dynamic modulus E is proportional to the resonance frequency f:

$$f = \frac{m^2 h}{2\pi\sqrt{12}L^2}\sqrt{\frac{E}{\rho}} \qquad (3)$$

where m is a constant ($m = 1.875$), ρ the material density, and L and h are the length and thickness of the sample, respectively.

3. Results and Discussion

Figure 2 shows the trends of Q^{-1} and E determined in MS tests carried out from room temperature to 466 K. Dynamic modulus monotonically decreases with temperature and the E *vs.* T curve can be fitted up to 418 K (Figure 3) by the polynomial relationship:

$$E = E_0\left(1 + b_1 T + b_2 T^2\right) \qquad (4)$$

where $E_0 = 12.76$ GPa is the modulus at room temperature, $b_1 = -1.02 \times 10^{-5}$ K^{-1} and $b_2 = -7.04 \times 10^{-7}$ K^{-2}. A second order polynomial function was chosen because the modulus behavior as temperature increases is certainly affected by two contributions: one due to anharmonicity, which leads to a linear decrease with T (first order term), and the other one to free electrons giving a contribution proportional to T^2 (second order term).

Above 418 K, as temperature approaches T_M, dynamic modulus exhibits an abrupt drop from 11.92 GPa to 8.50 GPa with a change of about 28%, while after melting it continues to decrease with nearly constant slope. Isothermal tests from 410 K to 440 K show the same modulus trend indicating that the huge drop is not an effect of the heating rate.
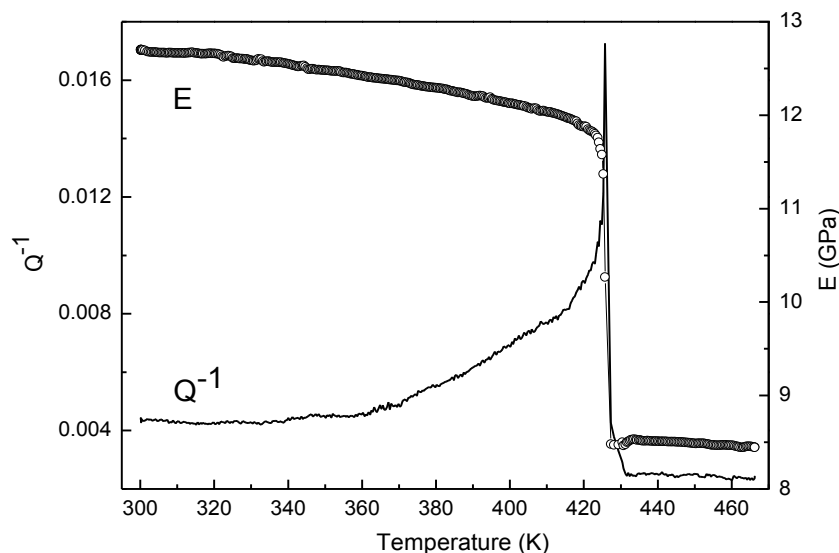
Figure 2. Q^{-1} and E trends of In from room temperature to 466 K.
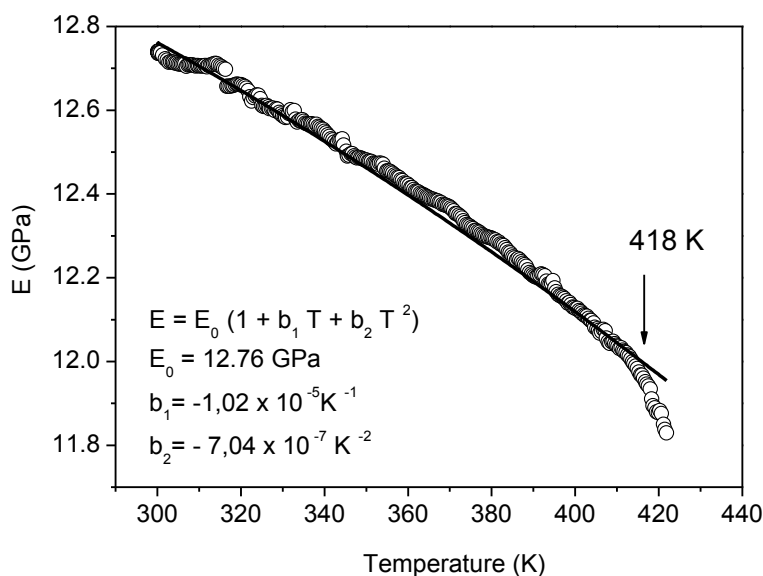

Figure 3. Dynamic modulus is fitted up to 418 K by Equation (4).

To explain the huge modulus drop above 418 K, other phenomena have to be taken into consideration together with anharmonicity and free electron contributions. In particular, the introduction of point defects could contribute to change the modulus through two different processes: dislocation pinning and diaelastic polarization of the defect strain field. However, since the samples have a very low density of dislocations, their pinning by point defects can be ruled out as the cause of the huge modulus change.

The diaelastic effect, *i.e.*, the fractional change of elastic modulus per concentration of point defects, could arise from both vacancies and self-interstitials. Vacancies are the predominant point defects in metals at elevated temperatures and most diffusion-mediated properties can be explained in terms of vacancy mechanisms [22] but there is clear evidence that the effect of vacancies on the elastic modulus of a solid is weak [23], whereas self-interstitials cause a large reduction [23]. The Granato theory [9] considers that melting is due to the thermo-activated increase in the interstitialcy

concentration (self-interstitials assuming the dumbbell configuration) and to their large compliance to the external shear stress that leads to big anelastic deformation in addition to the elasticity and, therefore, induces sharp reduction in modulus G to a small—but nonzero—quantity. The increase in the interstitialcy concentration C_I becomes extremely rapid just below T_M because of a decrease in the formation enthalpy with concentration and of the strong temperature dependence of formation entropy, as shown by Sinno *et al.* [14].

The close relationship of intersticialcy to melting has been confirmed by extensive computer simulations [24,25] and experiments [26,27]. In particular, Robrock and Schilling [27] measured a shear modulus G decrease of 27% and 19% for 1% defects in Al single crystals with <100> and <111> orientations, respectively. Such variations, ascribed by the investigators to self-interstitials with a <100> dumbbell configuration, are comparable with that observed by us. Therefore, the modulus drop seems consistent with a relevant increase of interstitialcy, as predicted by the Granato theory of melting.

The relevant Q^{-1} variation (from 8.0×10^{-3} to 1.7×10^{-2}) in correspondence to the modulus drop (Figure 2) supports this explanation. Owing to their dumbbell configuration, self-interstitials interact with the flexural vibration of samples and the periodic re-orientation under the external applied stress leads to energy loss and damping increase. The phenomenon has been extensively investigated for different types of point defect pairs and a lot of data can be found in the literature (e.g., see [15,16]).

When the solid–liquid (S-L) transformation has been completed, the dynamic modulus of the melt slowly decreases with temperature and its evolution is consistent with theoretical models for ideal monoatomic liquid metals, based on the assumption of spatial isotropy and two-body central interaction [28,29].

To correlate the MS results to structural changes, HT-XRD measurements have been carried out in the same temperature range. The XRD spectrum of set A samples recorded at T_M is the overlapping of the diffraction contributions of liquid and solid phases. As shown in Figure 4a, the two contributions have been separated by subtracting the pattern of liquid, obtained after completion of S-L transformation, to the overall spectrum. Contributions from solid and liquid have been then examined separately. This approach assumes that the shape of liquid contribution remains substantially unchanged after completion of the S-L transformation.

The RDF curve obtained from the liquid after the completion of S-L transformation is plotted in Figure 4b. It oscillates above and below the average density curve $4\pi r^2 \rho_0$. The vertical bars indicate the positions of 1st and 2nd neighbors in solid In. The RDF curve in Figure 4b exhibits the first peak centered at 3.3 Å. In is tetragonal body centered: the distance of 1st neighbors (4 atoms) is 3.25 Å and that of 2nd neighbors (8 atoms) is 3.38 Å. Therefore, shell radii of the 1st and 2nd neighbors in solid are very close to the mean distance of nearest neighbors in liquid.

The XRD contribution of the solid phase exhibits some important features, which are highlighted by the comparison with the spectrum recorded at 428 K, a temperature just below T_M (Figure 5).

First of all, the {101} reflection, absent in the spectrum at 428 K, appears at 429 K even if its intensity is relatively low. The presence of the {101} reflection involves a partial re-orientation of the grains in the solid, which accompanies or immediately precedes the formation of the first liquid. Moreover, the shape and position of the {002} peak change during melting; in fact, the peak remarkably shifts towards lower angles and broadens, in particular in the lower part.
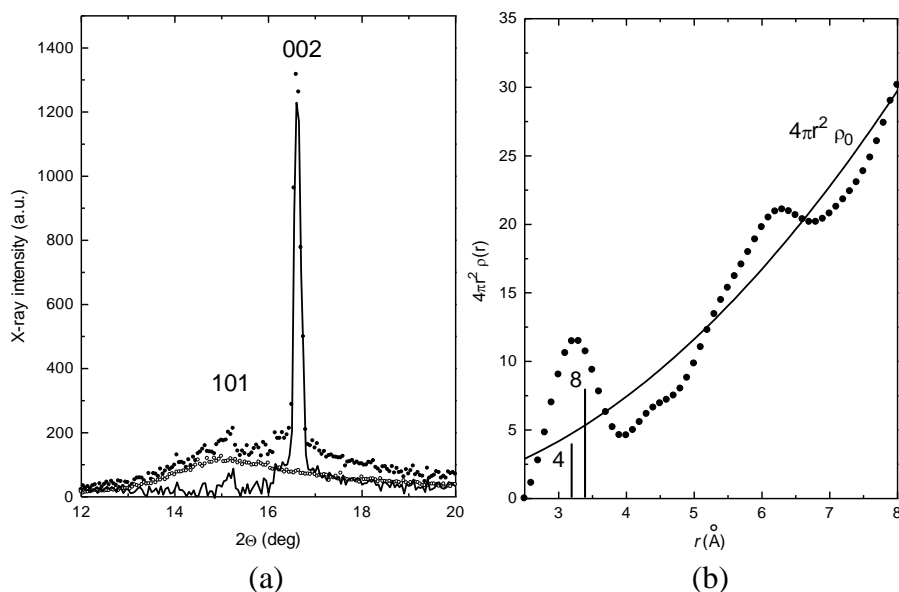
Figure 4. (**a**) The diffraction pattern of In (set A) collected during melting (black dots) is the sum of liquid (open circles) and solid (continuous line) contributions. (**b**) The RDF curve, $4\pi r^2 \rho(r)$ *vs.* r, obtained from the diffraction pattern after the completion of S-L transformation. Bars indicate the distribution of 1st and 2nd neighbors in crystalline In.

Samples of set B exhibit the same behavior: XRD spectrum shows only the {101} reflection up to 428 K and the {200} peak appears at 429 K.
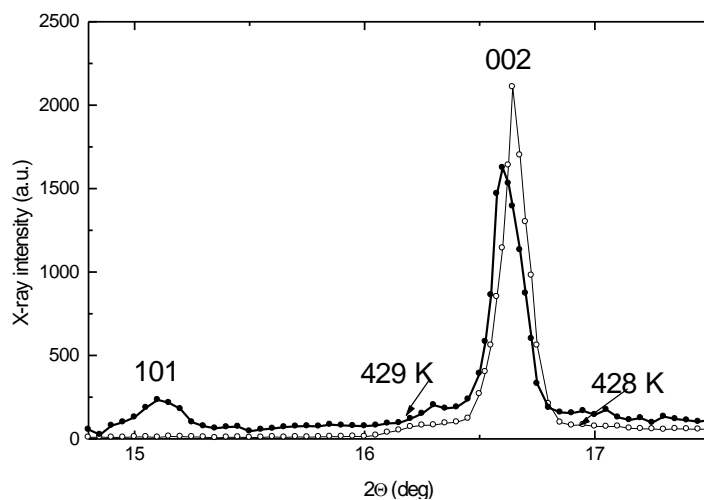

Figure 5. The XRD pattern of samples of set A recorded at 428 K, just below T_M, is compared with the contribution from solid to the overall pattern at 429 K.

The phenomena preceding and accompanying melting correspond to a fast structural evolution. On these grounds, the structure of both sets of samples has been monitored step by step by means of HT-XRD, starting from room temperature. For example, Figure 6 displays the {101} peak of set B samples at some increasing temperatures; as expected, the peak intensity progressively decreases and its central position shifts towards lower angles. The same behavior has been observed for the samples of set A.
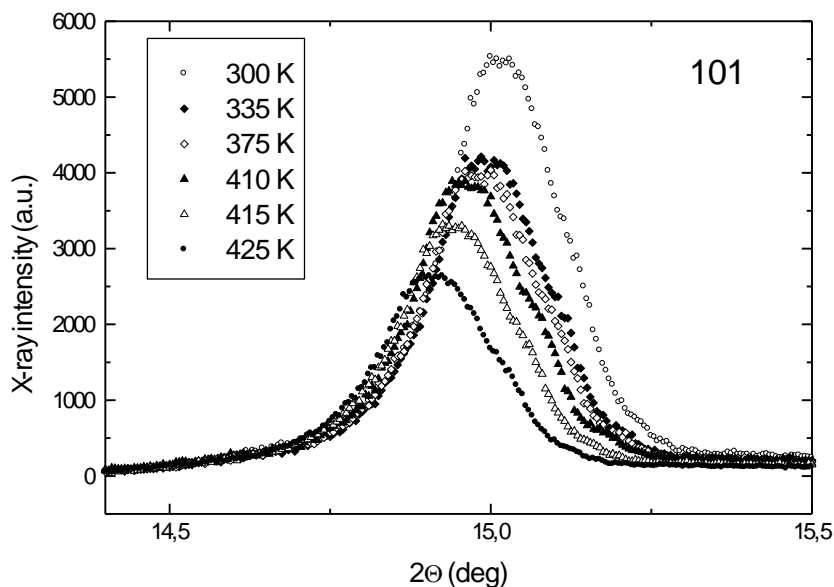
Figure 6. {101} XRD peak collected at increasing temperatures.

In both sets of samples the shift towards lower angles is progressive as temperature increases up to 428 K but at 429 K the peak position undergoes a most relevant change. Combining experimental data obtained from the samples of sets A and B, the lattice cell volume *V* has been calculated and its trend *vs.* temperature is displayed in Figure 7.

Graham *et al.* [30] investigated the thermal expansion of In and their data are fitted by the following empirical equations, which give the axis lengths *a* and *c*, expressed in Å, *vs.* the absolute temperature *T*:

$$a = 3.2182 + 8.47 \times 10^{-5}T + 3.61 \times 10^{-10}T^3 \tag{5}$$

$$c = 4.9201 + 15.15 \times 10^{-5}T - 6.64 \times 10^{-10}T^3 \tag{6}$$

The curve in Figure 7 shows a monotonous increase up to 428 K and its values are in good agreement with those determined from Equations (5) and (6), whereas at 429 K, the volume increase $\Delta V = 0.35$ Å^3 is outside the prediction based on the relationships of Graham *et al.* [30].
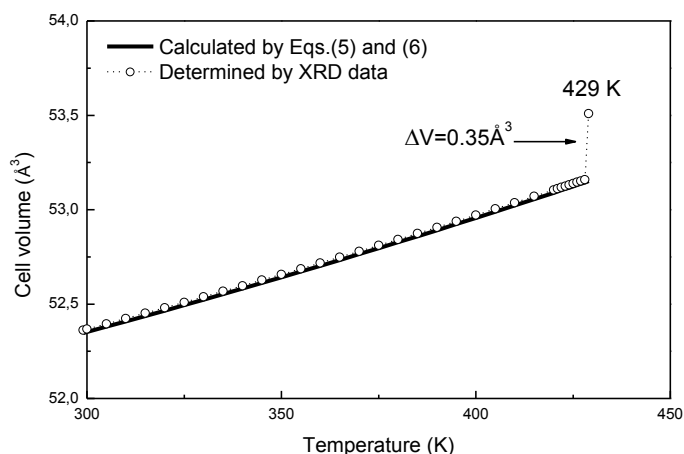

Figure 7. In cell volume *V vs.* temperature determined by XRD. The values calculated by Equations (5) and (6) are reported for comparison.

HT-XRD shows that lattice expansion *vs.* temperature is in good agreement with the empirical relationships of Graham *et al.* [30] up to 428 K; it diverges from such trend near T_M where a relevant cell volume increase ΔV is observed. This can be explained by an abrupt increase of vacancy concentration, which induce isotropic dilatation of crystal with a consequent increase of lattice spacings, evidenced by the shift of XRD reflections towards lower angles.

The vacancy concentration C_{429} at 429 K can be expressed as:

$$C_{429} = C_{428} + \Delta C \tag{7}$$

where C_{428} is the concentration of thermodynamic equilibrium at 428 K and ΔC the increase corresponding to the cell volume expansion ΔV shown in Figure 7. The value $\Delta C = 1.09 \times 10^{-2}$ has been estimated by the relative change of cell volume $\Delta V/V$ as:

$$\Delta C = \frac{\Delta V}{V} \Omega_{REL}^{-1} \tag{8}$$

where $\Omega_{REL} = -0.6$ (in atomic volume units) is the relaxed volume due to a single vacancy [31].

The vacancy concentration $C_{428} = 1.12 \times 10^{-4}$ has been determined by means of the relationship:

$$C = \exp(\frac{\Delta S}{k}).\exp(-\frac{\Delta H}{kT}) = \exp(-\frac{\Delta G}{kT}) \tag{9}$$

where $\Delta S = 6.90 \times 10^{-23}$ J K^{-1} [32] and $\Delta H = 8.33 \times 10^{-20}$ J [33] are, respectively, the activation entropy and enthalpy for the formation of a single vacancy; and $\Delta G = \Delta H - T \Delta S$ is the Gibbs free energy. Introducing into Equation (7) the values $C_{428} = 1.12 \times 10^{-4}$ and $\Delta C = 1.09 \times 10^{-2}$, the vacancy concentration C_{429} of the solid at the beginning of S-L transformation results to be $\approx 1.1 \times 10^{-2}$. Such huge vacancy concentration is consistent with the XRD results presented before. As shown in Figure 5, the {101} peak appears when the first liquid forms and indicates that a sudden grain re-orientation occurs in the solid phase. Due to the preliminary treatment, the examined material has a low dislocation density, therefore the driving force for recrystallization is low and the orientation change is ascribable to grain growth, made easier by the initial strong texture [34] and by the enhancement of boundary mobility due to vacancy flux or supersaturation, as extensively discussed in the literature (e.g., see [35]).

The huge increase of vacancies at T_M involves also extremely favorable conditions for vacancy aggregation to form complex defects. The broadening of XRD peaks, in particular in their lower part and along the tails, is consistent to vacancy clustering in small dislocation loops. This type of defect produces a diffuse scattering, which affects the tails of diffraction profiles [36,37]. Unfortunately, the conditions of present experiments do not allow quantitative evaluations of density and mean radius of dislocation loops.

The results of this work indicate that self-interstitials and vacancies play a synergic role in metal melting. The high concentration of self-interstitials causes a weakening of interatomic bonds testified by the elastic modulus drop. The process begins at about 418 K while an abnormal increase of vacancy concentration occurs at 429 K, immediately before and during melting. Therefore, it is supposed that the weakening of interatomic bonds induced by self-interstitials diminishes the vacancy formation

energy and determines extremely favorable conditions for the huge vacancy increase that leads to the final lattice collapse and melting.

4. Conclusions

Precursor effects of indium melting have been investigated by means of Mechanical Spectroscopy (MS) and High Temperature X-ray Diffraction (HT-XRD).

MS showed dynamic modulus drop of about 28% when temperature approaches the melting point. Such changes, which is accompanied by a corresponding variation of damping, occurs in the temperature range 418–429 K and, according to the Granato theory, can be explained by a concentration increase of interstitialcies (self-interstitials with a dumbbell configuration).

A further contribution to the knowledge of the microstructural evolution before and during melting was provided by HT-XRD showing partial grain re-orientation, peak profile broadening, in particular in the lower part, and peak shift towards lower angles. These phenomena indicate a remarkable increase of vacancy concentration, which has been estimated to be of the order of $\approx 10^{-2}$ at 429 K.

It is concluded that both vacancies and self-interstitials play an important role in melting. The increase of self-interstitials that takes place in a temperature range of about 10 K before melting weakens interatomic bonds as demonstrated by modulus reduction and favors the final avalanche of vacancies leading to the S-L transformation.

Author Contributions

R.Montanari and A. Varone conceived and designed the experiments; R.Montanari and A. Varone performed the experiments; R.Montanari and A. Varone analyzed the data; R.Montanari and A. Varone wrote the paper.

Conflicts of Interest

The authors declare no conflict of interest.

References

1. Ubbelohde, A.R. *The Molten State of Matter-Melting and Crystal Structure*; Wiley Interscienceublication: New York, NY, USA, 1979.
2. Lindemann, F. Uber die Berechnung molekularer Eigenfrequenzen. *Phys. Z.* **1910**, *11*, 609–612.
3. Born, M. Thermodynamics of Crystals and Melting. *J. Chem. Phys.* **1939**, *7*, 591–603.
4. Hunter, L.; Siegel, S. The Variation with Temperature of the Principal Elastic Moduli of NaCl near the Melting Point. *Phys. Rev.* **1942**, *61*, 84–95.

5. Tallon, J.L. The volume dependence of elastic moduli and the Born-Durand melting hypothesis. *Philos. Mag. A* **1978**, *39*, 151–161.

6. Gorecki, T. Vacancies and changes of physical properties of metals at the melting point. *Z. Metall.* **1974**, *65*, 426–431.

7. Kuhlmann-Wilsdorf, D. Theory of melting. *Phys. Rev.* **1965**, *140*, A1599–A1610.

8. Weber, T.A.; Stillinger, F.H. Inherent structures and distribution functions for liquids that freeze into bcc crystals. *J. Chem. Phys.* **1984**, *81*, 5089–5094.

9. Granato, A.V. Interstitialcy model for condensed matter states of face-centered-cubic metals. *Phys. Rev. Lett.* **1992**, *68*, 974–977.

10. Jin, Z.H.; Gumbsch, P.; Lu, K.; Ma, E. Melting Mechanisms at the Limit of Superheating. *Phys. Rev. Lett.* **2001**, *87*, doi:10.1103/PhysRevLett.87.055703.

11. Gomez, L.; Dobry, A.; Diep, H.T. Monte Carlo simulation of the role of defects as a melting mechanism. *Phys. Rev. B* **2001**, *63*, doi:10.1103/PhysRevB.63.224103.

12. Gomez, L.; Dobry, A.; Geuting, Ch.; Diep, H.T.; Burakovsky, L. Dislocation Lines as the Precursor of the Melting of Crystalline Solids Observed in Monte Carlo Simulations. *Phys. Rev. Lett.* **2003**, *90*, doi:10.1103/PhysRevLett.90.095701.

13. Lutsko, J.F.; Wolf, D.; Phillpot, S.R.; Yip, S. Molecular-dynamics study of lattice-defect-nucleated melting in metals using an embedded-atom-method potential. *Phys. Rev. B* **1989**, *40*, 2841–2855.

14. Sinno, T.; Jiang, Z.K.; Brown, R.A. Atomistic Simulation of High-Temperature Point Defect Properties in Crystalline Silicon. *Appl. Phys. Lett.* **1996**, *68*, 3028–3031.

15. Nowick, A.S.; Berry, B.S. *Anelastic Relaxation in Crystalline Solids*; Academic Press: New York, NY, USA; London, UK, 1972.

16. Blanter, M.S.; Golovin, I.S.; Neuhauser, H.; Sinning, H.-R. *Internal Friction in Metallic Materials—A Handbook*; Springer Verlag: Berlin, Germany; Heidelberg, Germany, 2007.

17. Zhu, Z.G.; Zu, F.Q.; Guo, L.J.; Zhang, B. Internal friction method: Suitable also for structural changes of liquids. *Mater. Sci. Eng. A* **2004**, *370*, 427–430.

18. Deodati, P.; Gauzzi, F.; Montanari, R.; Varone, A. Structural Changes of Liquid Pb-Bi Eutectic Alloy. *Mater. Sci. Forum* **2012**, *706–709*, 878–883.

19. Montanari, R.; Varone, A. Mechanical Spectroscopy Investigation of Liquid Pb-Bi Alloys. *Solid State Phenom.* **2012**, *184*, 434–439.

20. Montanari, R. Real-time XRD investigations on metallic melts. *Int. J. Mater. Prod. Technol.* **2004**, *20*, 452–463.

21. Amadori, S.; Campari, E.G.; Fiorini, A.L.; Montanari, R.; Pasquini, L.; Savini, L.; Bonetti, E. Automated resonant vibrating reed analyzer apparatus for a non destructive characterization of materials for industrial applications. *Mater. Sci. Eng. A* **2006**, *442*, 543–546.

22. Siegel, R.W. Vacancy concentrations in metals. *J. Nucl. Mater.* **1978**, *69–70*, 117–146.

23. Kanigel, A.; Adler, J.; Polturak, E. Influence of point defects on the shear elastic coefficients and on the melting temperature of copper. *Int. J. Mod. Phys. C* **2001**, *12*, 727–737.

24. Nordlund, K.; Averback, R.S. Role of Self-Interstitial Atoms on the High Temperature Properties of Metals. *Phys. Rev. Lett.* **1998**, *80*, 4201–4204.

25. Forsblom, M.; Grimvall, G. How superheated crystals melt. *Nat. Mater.* **2005**, *4*, 388–390.

26. Gordon, C.A.; Granato, A.V. Equilibrium concentration of interstitials in aluminum just below the melting temperature. *Mater. Sci. Eng. A* **2004**, *370*, 83–87.

27. Robrock, K.H.; Schilling, W. Diaelastic modulus change of aluminium after low-temperature electron-irradiation. *J. Phys. F Met. Phys.* **1976**, *6*, 303–314.

28. Nemilov, S.V. Interrelation between shear modulus and the molecular parameters of viscous flow for glass forming liquids. *J. Non-Cryst. Solids* **2006**, *352*, 2715–2725.

29. Knuyt, G.; de Schepper, L.; Stals, L.M. Calculation of some metallic glass properties, based on the use of a Gaussian distribution for the nearest-neighbour distance. *Philos. Mag. B* **1990**, *61*, 965–988.

30. Graham, J.; Moore, A.; Raynor, G.V. The effect of temperature on the lattice spacings of indium. *J. Inst. Met.* **1955**, *84*, 86–87.

31. Dickman, J.E.; Jeffrey, R.N.; Gustafson, D.R. Vacancy formation volume in indium from positron-annihilation measurements. *Phys. Rev. B* **1977**, *16*, 3334–3337.

32. Weiler, W.; Schaefer, H.E. Vacancy formation in indium investigated by positron lifetime spectroscopy. *J. Phys. F Met. Phys.* **1985**, *15*, 1651–1659.

33. In *Atomic Defects in Metals*; Ehrhart, P., Jung, P., Schultz, H., Ullmaier, H., Eds.; Landoldt-Bornstein—Group III Condensed Matter Series 25; Spriger-Verlag: Berlin, Germany; Heidelberg, Germany, 1991.

34. Humphreys, F.J.; Hatherly, M. *Recrystallization and Related Annealing Phenomena*; Pergamon Press: Oxford, UK, 1996.

35. In *Recrystallization of Metallic Materials*; Haessner, F., Hofman, S., Eds.; Dr. Riederer Verlag: Stuttgart, Germany, 1978.

36. Dederichs, P.H. Diffuse Scattering from Defect Clusters near Bragg Reflections. *Phys. Rev. B* **1971**, *4*, 1041–1050.

37. Bonetti, E.; Fuschini, E.; Montanari, R.; Servidori, M.; Uguzzoni, A. X-ray diffraction study on proton-irradiated high-purity aluminum. *Mater. Lett.* **1989**, *8*, 477–480.